machines

MDPI

Article

Process Window Based on Vibration and Torque for Dry Disc Milling of Thick Steam Generator Shells in Nuclear Decommissioning

Jozef Varga [1,*], Ján Semjon [2], Patrik Pilát [1], Boris Jobbágy [1] and Ondrej Šimko [1]

[1] Prototyping and Innovation Centre, Faculty of Mechanical Engineering, Technical University of Košice, Letná 9, 040 01 Kosice, Slovakia; patrik.pilat@tuke.sk (P.P.); boris.jobbagy@tuke.sk (B.J.); ondrej.simko@tuke.sk (O.Š.)
[2] Department of Production Systems and Robotics, Faculty of Mechanical Engineering, Technical University of Košice, Letná 9, 040 01 Kosice, Slovakia; jan.semjon@tuke.sk
* Correspondence: jozef.varga.2@tuke.sk

Abstract

Dry disc milling cuts thick carbon-steel components in nuclear decommissioning without liquid waste, but no catalogue gives a safe spindle speed and feed for a large remote module. This paper sets out an application-specific procedure for the longitudinal module on the 75 mm shell of a VVER-440 steam generator. A portable analyser and the drive log are the only measurements. Vibration depends on spindle speed, and torque depends on feed per revolution. Seven velocity spectra (60–120 rpm) were recorded on a test stand. Torque comes from 599 records of the module installed in the cell. At 80 rpm a 690–780 Hz band reaches 3.47 mm/s. Order tracking is consistent with a speed-locked order crossing a fixed band; the natural frequency was not measured. At 110 rpm the band is 0.22 mm/s, the lowest value of that sweep for five band definitions. In 65 cuts at 90 rpm and 2 mm/s, the mean torque is 11.3 N·m and the 99th percentile is 26.4 N·m. The mean matches the supplier's calculation at that one condition. A 45 N·m limit on the 99th percentile—taken only from jam precursors on an earlier thinner (35 mm) cut, not from the 75 mm wall of the window—gives a model-predicted condition at 110 rpm and 240 mm/min: a kinematic removal rate of 108 cm^3/min, twice current practice, and 56% less test-stand vibration than at 90 rpm. The torque at 110 rpm is extrapolated, and that point has not been cut. The speed remains 110–120 rpm in all 36 sensitivity cases. Doubling the removal rate requires the 45 N·m limit.

Keywords: disc milling; process window; spindle drive torque; vibration spectrum; order analysis; Kienzle model; nuclear decommissioning; VVER-440

Check for updates

Academic Editor: Yuwen Sun

Received: 9 October 2026
Revised: 26 October 2026
Accepted: 3 November 2026
Published: 5 November 2026

Copyright: © 2026 by the authors. Licensee MDPI, Basel, Switzerland. This article is an open access article distributed under the terms and conditions of the Creative Commons Attribution (CC BY) license.

1. Introduction

Several hundred power reactors will be dismantled over the next decades [1], and segmentation of thick, activated or contaminated steel components is one of the main cost and dose drivers of that work [2,3]. For steam generators, the cutting sequence and the time spent near the component determine the collective dose of the dismantling crew [4], and the choice among cutting technologies is itself a multi-criteria decision [5]. Thermal and abrasive-water-jet cutting are fast but produce aerosols, slag or a large volume of secondary waste [2]. Mechanical cutting with a narrow disc mill produces a solid chip that can be collected; done dry, it also avoids contaminated coolant [6,7]. Its load is bounded by the spindle drive, which makes it suitable for a remotely operated module. The operator still

has to choose the spindle speed n and the feed v_f. On this large, compliant structure, the supplier provides a cutting-power check, but no stability limit and no load limit.

Machining science treats the two limits that matter here separately. Self-excited (regenerative) chatter in milling is reviewed by Zhu and Liu [8]; the classical machine-tool formulation is that of Merritt [9]. For milling it is predicted by frequency-domain stability lobes [10,11] and by time-domain discretisation methods [12,13]; intermittent, low-immersion cutting needs multi-frequency solutions [14,15]. Reviews and textbooks summarise the field [16,17], and recent work concentrates on signal-based detection and classification of chatter [18]. All prediction methods need the frequency-response function at the tool and the cutting coefficients. On a large, one-off machine, the structural dynamics also change with position and process [19]. They can be estimated in operation [20,21], but this is rarely done for decommissioning equipment. The closest industrial analogue, large band and circular sawing, is likewise treated empirically [22].

Cutting load follows from chip mechanics [23] and is estimated in practice with specific-force models, classically the Kienzle–Victor law [24], or with mechanistic coefficients identified from tests [25,26]. Because a servo drive must supply that load, the motor current or torque is itself a force sensor [27,28]. It has been used to detect chatter [29,30] and, more broadly, for process and tool-condition monitoring [31,32]. Parameter selection then trades such constraints against tool life, productivity or energy [33,34].

Published methods do not by themselves choose n and v_f for a one-off decommissioning module. Stability lobes need the frequency-response function at the tool [10,16]. Feed-current methods were developed for machining centres [27,28]. Monitoring reviews describe detection and tool condition, rather than a cutting window [31,32]. Tool-life and energy criteria do not consider structural resonance [33,34]. Studies of large saws are empirical and stop at detection [22]. Table 1 places these approaches next to the procedure used here.

Table 1. Methods cited above, and what each of them does not supply for the longitudinal module. The check column is what those studies measured.

Study	Signal	Aim	Check	Not Provided for This Module
Altintas and Budak, [10]	tool FRF, force coefficients	chatter-free speed	cutting tests	an FRF measured on this module
Altintas, [27]; Kim and Kim, [28]	feed-drive current	cutting force	machining-centre tests	this spindle and this disc
Teti et al., [31]	several sensors	process monitoring	review	a window in (n, v_f)
Taylor, [33]; Kara and Li, [34]	tool life or power	life or energy	workshop data	a structural resonance
Thaler et al., [22]	sound	chatter detection in sawing	an industrial saw	a choice of speed and feed
This paper	one accelerometer, drive log	feasible (n, v_f)	test-stand sweep; log at 90 rpm	a cut at the predicted point

The field procedure still missing from that list uses only a portable analyser and the drive log, and it keeps the two limits apart. Structural vibration depends on n. Drive-train load depends on chip thickness, and hence on v_f/n. This paper applies that procedure to the fragmentation cell that segmented the twelve VVER-440 steam generators at Jaslovské Bohunice V1 [35,36]. The cell builds on earlier mobile fragmentation systems [37] and is described in European patent application EP 3 984 674 A1 [38]. The contribution is an

engineering procedure for this module, cutter and wall. It is not a new theory of chatter, and it is not a new cutting-force law. The procedure contains four parts: (i) a resonant-band metric whose speed ranking does not change with the band limits, together with an order analysis of the speed-locked component; (ii) a torque model fitted to steady segments of the production log, with separate exponents for the mean and the 99th percentile, and a level check against the supplier's cutting-power calculation; (iii) thermal and peak limits taken from the motor data sheet, the gearbox data sheet and the recorded jams; and (iv) a ranked (n, v_f) window, recomputed for 36 sensitivity cases. The pair named below is a model-predicted feasible condition. It has not been run.

2. Materials and Methods

2.1. Cutting Module, Tool and Drives

The PGV-4E steam generator is a horizontal vessel with a shell diameter of about 3.2 m and wall thicknesses of 75 mm and 135–140 mm. The cell (StarGate) carries its cutting modules on a closed ring guide around the shell, and the cutter is fed into the cut by a wedge mechanism on pre-tensioned rolling elements [36,38]. With this cell, one 140 t generator was segmented in 45 days, and all twelve were finished in 2023 [36]. This paper concerns the 75 mm wall, which is cut by the longitudinal module (Figure 1). Its cutter is an ISCAR side-slotting disc mill with $D_C = 420$ mm, cutting width 6 mm, $z = 28$, lead angle 90° and effective rake 10°, as stated in the supplier's cutting-power calculation for this cut (an unpublished ISCAR report provided with the tool). The wall is GOST 22K boiler steel [39], a normalised low-carbon grade that corresponds to AISI 1020–1023.



Figure 1. Longitudinal cutting module (yellow) on the ring frame of the fragmentation cell, positioned on the shell of a VVER-440 (PGV-4E) steam generator; the tube bundle is visible inside the shell [38].

Table 2 lists the drives. The spindle motor is a B&R 8LSA77.R2030D000-3 permanent-magnet synchronous servo motor: nominal speed 3000 rpm, nominal torque $M_n = 40$ N·m, stall torque $M_0 = 73$ N·m, peak torque $M_{max} = 270$ N·m, maximum speed 4500 rpm [40]. The design documentation of the cell quotes 50 N·m; the data-sheet values are used here. The motor drives the cutter through an Apex Dynamics AP200 two-stage high-torque planetary gearbox (Table 3) [41]. The ratio $i = 28$ is one of the standard catalogue ratios of the two-stage AP200. Motor torque is referred to the cutter by $i \cdot \eta = 26.3$. That product is the ratio times the efficiency, not a second value of i. All motor-side quantities used for the window (T_m, T_{lim} and the vibration metric) are independent of i; only the cutter-side torques in

Table 3, the motor speeds and the comparison with the supplier's calculation scale with it. The catalogue efficiency of a two-stage AP200, at least 94%, is the value of η used throughout. Thus 90 rpm at the cutter is 2520 rpm at the motor, and 110 rpm is 3080 rpm. Both are below the gearbox's nominal input speed of 3700 rpm and its maximum of 5500 rpm. The motor nominal speed is 3000 rpm and its maximum is 4500 rpm, so 3080 rpm at the motor remains on the motor characteristic [40]. All axes run in speed control, so n is held constant and T_m varies to hold it.

Table 2. Drives of the longitudinal cutting module (design documentation of the cell). Spindle motor ratings from [40]. T_m in this paper is the motor-side torque of the 8LSA77; the gearbox output (cutter) torque is $T_m\, i\, \eta = 26.3\, T_m$.

Function	Motor (B&R)	Transmission	M_n (N·m)	Remark
Cutter spindle	8LSA77.R2030D000-3	Apex AP200, 2-stage planetary, $i = 28$	40	n_N 3000 rpm, M_0 73 N·m, M_{max} 270 N·m, n_{max} 4500 rpm [40]
Feed in the cut	8LSA45.R2030D200-3	$i = 2$ + ball screw D40 × 5	6.16	set-points 1–4 mm/s
Infeed into the cut	8LSA45.R2030D200-3	$i = 2$ + ball screw D40 × 5	6.16	0.1–0.5 mm/s; depth held ±5 mm
Module travel on guide (pair)	8LSA46.R2030D200-3	$i = 60$	6.8	positioning only
Frame travel on rails (pair)	8LSA55.R2030D200-3	$i = 60$	11.6	5 and 10 mm/s

Table 3. Catalogue data of the Apex Dynamics AP200 spindle gearbox [41] and the loads imposed by the model-predicted point. Cutter-side values scale with i.

Quantity (AP200, Two-Stage)	Catalogue Value	Load in This Study (Cutter Side)
Nominal output torque T_{2N}	2015 N·m ($i = 28$)	mean torque 16.3 N·m × 26.3 = 428 N·m (21% of T_{2N})
Max. acceleration torque $T_{2B} = 1.5\, T_{2N}$	3022 N·m	$T_{m,99}$ = 45 N·m → 1184 N·m (39% of T_{2B})
Emergency-stop torque $T_{2NOT} = 3\, T_{2N}$	6045 N·m	highest jam torque 68 N·m → 1790 N·m (30% of T_{2NOT})
Nominal/max. input speed	3700/5500 rpm	2520 rpm (90 rpm), 3080 rpm (110 rpm)
Efficiency	≥94%	$\eta = 0.94$ used in all conversions

Backlash, torsional rigidity, the allowable bending moment and the IP67 rating are given in the same catalogue. They do not enter the window, so they are omitted here.

The supplier's cutting-power calculation for this cut is summarised in Table 4. At $f_z = 0.1$ mm and $n = 90.9$ rpm ($v_c = 120$ m/min, $v_f = 254.5$ mm/min), it predicts a specific cutting force of 2245 N/mm^2 at $h_m = 0.041$ mm. The predicted net power is 4.29 kW and the mean and maximum torques at the cutter are 450 and 558 N·m. The report gives no recommended cutting-speed range. These values are used in Section 2.4 as a consistency check of the measured torque.

Table 4. ISCAR Machining Power calculation for side slotting with the 420 mm, 28-tooth disc mill (supplier's report, unpublished).

Input	Value	Output	Value
Cutting diameter D_C	420 mm	Specific cutting force K_c	2245 N/mm^2
Radial depth a_e	75 mm	Net mean power	4.29 kW

Table 4. *Cont.*

Input	Value	Output	Value
Effective edges z	28	Material-removal rate	114.5 cm^3/min
Feed per tooth f_z	0.1 mm	Average chip thickness h_m	0.0409 mm
Cutting width CW	6 mm	Mean torque (cutter)	450.4 N·m
Cutting speed v_c/ n	120 m/min/90.9 rpm	Max. torque (cutter)	557.5 N·m
Material	AISI 1020–1023	Max. spindle bending force	2895 N

2.2. Vibration Measurement

The first version of the longitudinal module was mounted on a test stand and cut a 75 mm steel plate (Figure 2). Vibration was recorded on 23 November 2018 with an Adash A4400 VA4 Pro portable analyser in recorder mode [42]. One accelerometer was connected to input AC1 and oriented in the X direction of the module; the analyser also displayed the spindle speed. The seven speeds were run within one session of 4.3 min (15:12:43–15:17:02) under one unchanged feed programme. The feed was not logged, so the records form a speed series at one feed programme. Only the X direction was recorded, with one accelerometer. Each spectrum used below is a single 0.25 s block from that one session. The sweep therefore supports a comparative ranking. It does not support a standard deviation or a claim of statistical repeatability. The time records are 21–43 s long, and the analyser's input range was set between ±2 g and ±6 g.

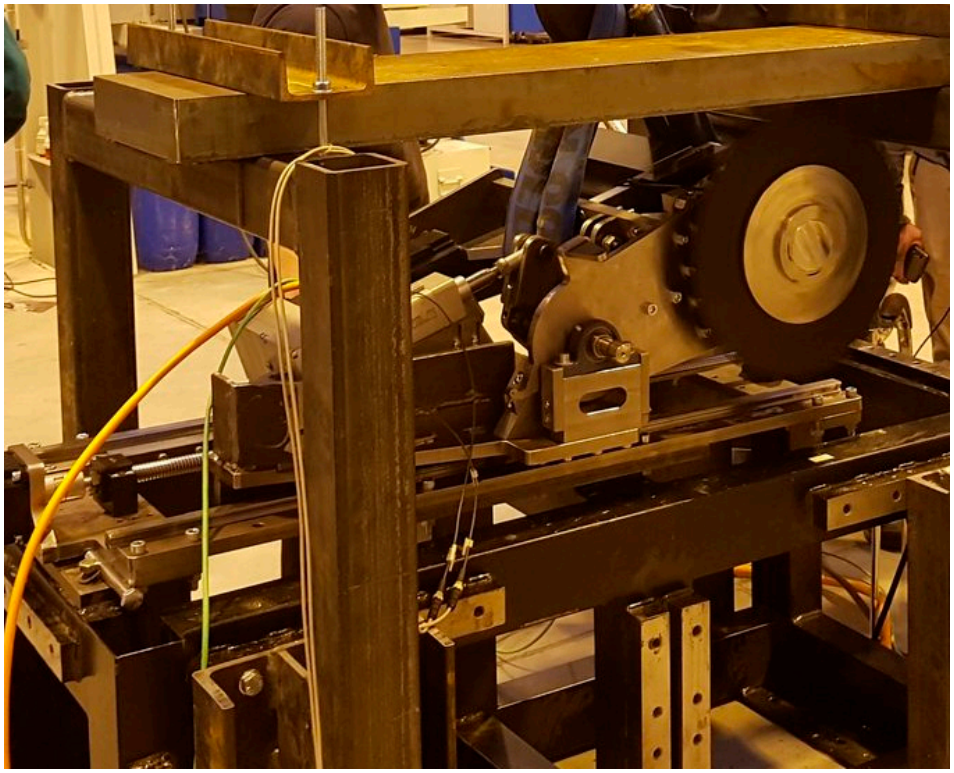

Figure 2. Longitudinal cutting module (first version) on the test stand used for the vibration sweep.

For each speed the analyser computed a velocity spectrum from a 0.25 s block of the time record, 10–6400 Hz with 1600 lines (4 Hz resolution) and a Hanning window, and exported it with 1601 values in mm/s RMS. Figure 3 shows two of the analyser screens. Two scalars

are extracted from each spectrum $A(f)$: the dominant-line amplitude $A_{\text{peak}} = \max A(f)$, and the resonant-band metric

$$A_{\text{band}} = \sqrt{\frac{1}{1.5} \sum_{f \in [690,\ 780]\ \text{Hz}} A^2(f)} \tag{1}$$

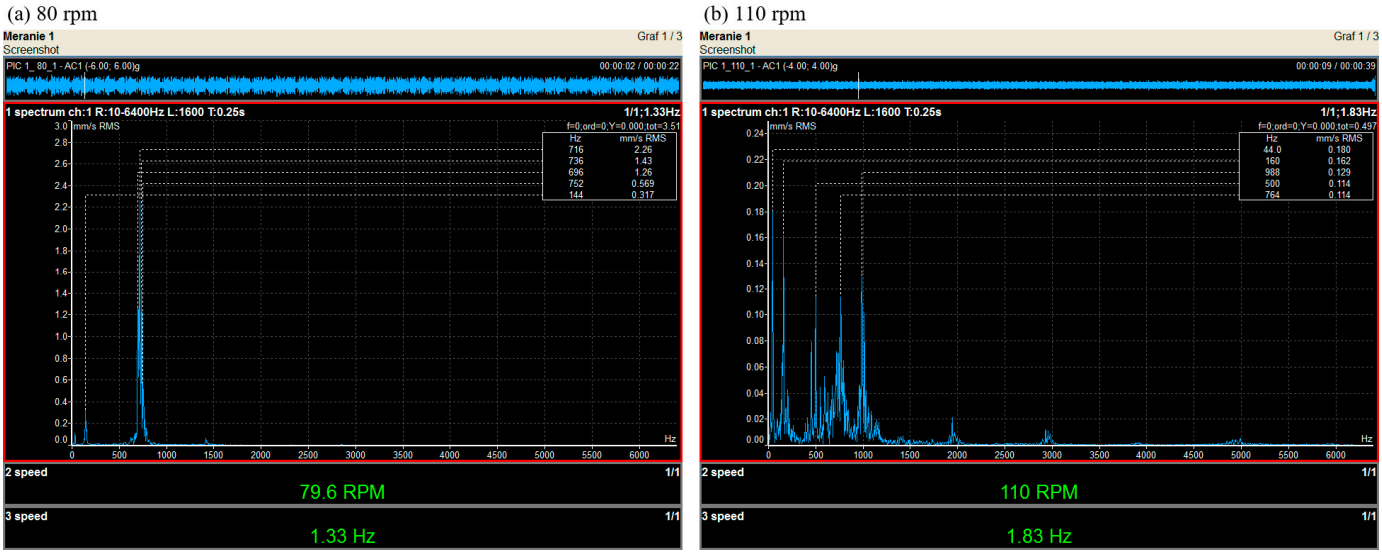

Figure 3. Original analyser screens recorded by the authors during the vibration sweep of this study (Adash A4400 VA4 Pro): (**a**) 80 rpm, (**b**) 110 rpm. Top strip: acceleration time record (channel AC1); centre: velocity spectrum 10–6400 Hz, 1600 lines, 0.25 s block, with the five largest lines and the overall value (tot); bottom: spindle speed.

The factor 1/1.5 is the equivalent noise bandwidth of the Hanning window, which spreads each spectral component over several lines; without it, the root-sum-square over lines over-estimates the RMS by a factor of $\sqrt{1.5}$ [43]. With the correction, the broadband value over 10–6400 Hz reproduces the analyser's own overall value within 0.5% at six speeds and within 3% at 60 rpm (Table 5), which verifies the window and the scaling. Figures 4 and 5 are plotted in software from these exported lines. Figure 3 is the analyser screen itself, kept so the export can be checked against the instrument. A_{band} is a comparative quantity in the spirit of band-limited condition-monitoring indicators [44]. It is not an overall value in the sense of ISO 20816-3 [45]; the standard is used only as a scale. Its sensitivity to the band limits is examined in Section 3.1.

Table 5. Band RMS of the velocity spectra (mm/s), Equation (1) with the Hanning correction, for five band definitions; broadband over 10–6400 Hz; analyser total = overall value displayed by the A4400 (Figure 3).

n (rpm)	A_{band} 690–780	680–790	700–760	650–800	600–900	Broadband 10–6400	Analyser Total
60	0.56	0.57	0.55	0.58	0.58	0.66	0.68
70	0.67	0.68	0.40	0.70	0.91	1.00	1.00
80	3.47	3.48	3.28	3.48	3.49	3.51	3.51
90	0.51	1.01	0.36	1.13	1.28	1.40	1.40
100	0.39	0.39	0.36	0.40	0.54	0.67	0.67
110	0.22	0.23	0.18	0.25	0.27	0.50	0.50
120	0.30	0.32	0.25	0.34	0.36	0.57	0.57

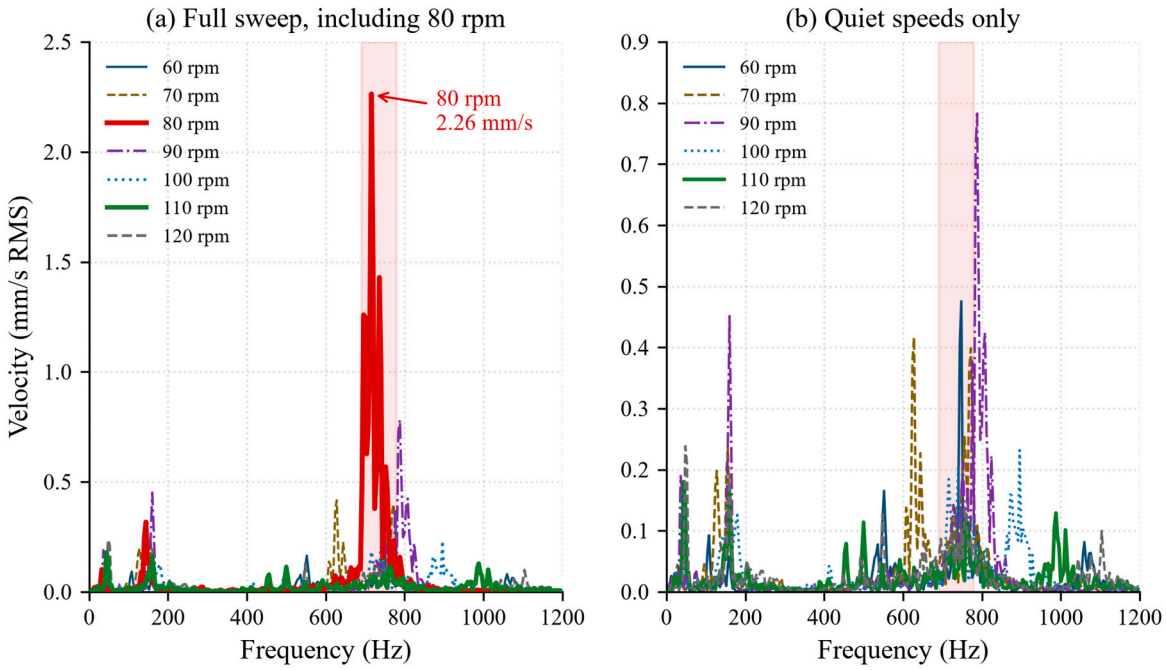

Figure 4. Velocity spectra of the speed sweep (0–1200 Hz, plotted from the exported lines, with a separate colour and line style for each speed). (**a**) All seven speeds; the 80 rpm cluster at 716 Hz dominates. (**b**) Without 80 rpm, so that the quiet records remain readable. Shading: band of Equation (1).

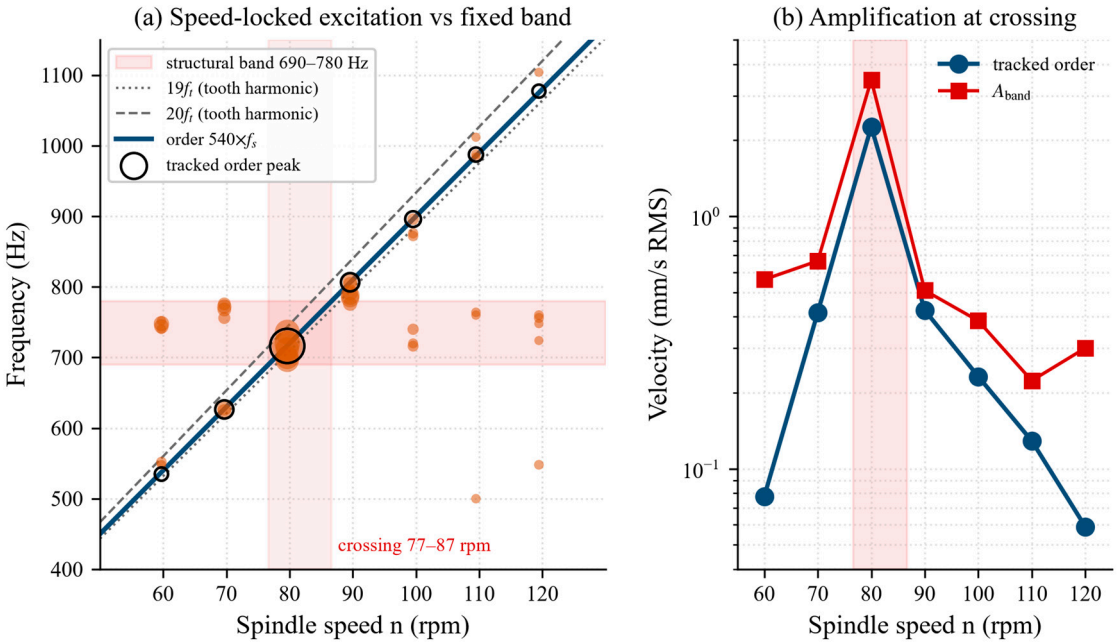

Figure 5. Order analysis, plotted from the exported spectra. (**a**) Frequencies of the six strongest lines in 400–1150 Hz at each speed (orange, area proportional to amplitude), the tracked order 540 f_s (navy; circles: tracked peaks), the tooth harmonics 19 f_t and 20 f_t (grey) and the band of Equation (1). (**b**) Amplitude of the tracked order and A_{band} versus speed; shading: speed interval in which the order lies in the band.

2.3. Drive Log and Segmentation

The PLC of the assembled cell streamed all drive signals to ibaPDA at 100 Hz. The archive contains 599 records of 10 min each (April–December 2019). The proprietary DAT format (run-length-encoded payload with XOR-masked channel offsets) was decoded with

a purpose-written reader, and the decoded traces were checked against ibaAnalyzer plots of the same records. For each record the reader extracts spindle speed and torque, the feed and infeed speeds (mm/s) and the axis torques. A steady segment is a run of at least 5 s in which the rounded spindle speed, feed set-point and infeed set-point are constant; the first second is discarded. For each segment the mean, median, 95th and 99th percentiles and the maximum of T_m are stored. The procedure yields 424 segments. All loaded cutting took place at 90 rpm; other speeds appear only as ramps. Feed set-points are discrete: 1, 2, 3 and 4 mm/s, plus 10–20 mm/s rapid moves.

Not every loaded segment is comparable. The 3 mm/s cuts of April 2019 belong to an internal mock-up test with a 540 mm cutter at 65 mm depth, and the 1 mm/s cuts of April–July 2019 were made on a thinner (35 mm) wall (operating records of the cell). Both are excluded from the identification of the 75 mm window; the 35 mm thickness is not a second target. The reference set comprises the cuts of the 75 mm wall by the longitudinal module on 5 June and 16 December 2019 at 90 rpm and 2 mm/s (120 mm/min), the production setting for this wall: 65 segments, 2064 s of cutting.

Spindle stops during cutting were classified from the speed trace. Five stops are jams. All five belong to that thinner-wall jam dataset (35 mm, 1.0–1.2 mm/s), not to the 75 mm cuts that define the process window: the torque rose while n was still 90 rpm, and the speed then collapsed to zero within one 10 ms sample (within 1 s in one record). The torques immediately before the collapse were 49.3, 63.8, 64.6, 65.7 and 68.2 N·m (median 64.6 N·m). Nine further stops, all on the 75 mm wall, were controlled stops: the speed fell along a linear ramp from 85 to 40 rpm in 0.53–0.60 s with 0.8–6.2 N·m during deceleration, the feed stopped at the same instant, and in several records the spindle returned to 90 rpm afterwards. The torque before these stops was 20–50 N·m. No jam was recorded on the 75 mm wall, although isolated peaks of about 50 N·m occurred there.

2.4. Torque Model and Consistency Check

For peripheral slitting with engagement angle $\varphi = \arccos(1 - a_e/R)$, $R = D_C/2$, the mean uncut chip thickness is $h_m = f_z\, a_e/(R\,\varphi)$ with $f_z = v_f/(n\,z)$ [16]. With the Kienzle law $k_c = k_{c1.1}\, h_m^{-m_c}$, the cutting power is $P_c = k_c\, a_e\, a_p\, v_f$ and the motor torque is $T_m = P_c/(i\,\eta\,\omega)$ [24]. At fixed geometry this reduces to

$$T_m - T_0 \propto \left(\frac{v_f}{n}\right)^e, \quad e = 1 - m_c \tag{2}$$

that is, $T_m - T_0 = C\,(v_f/n)^e$. The constant C collects $k_{c1.1}$, the cut geometry (a_e, a_p, D_C, z) and the drive constants i and η, which do not change during a cut. Torque therefore depends only on the feed per spindle revolution $v_f/\,n$; with the usual $m_c = 0.25$, $e = 0.75$. The supplier's calculation (Table 4) gives an absolute value for comparison. Its mean cutter torque, 450 N·m, is 17.1 N·m on the motor side. Scaled with Equation (2) from $v_f/\,n = 2.8$ mm/rev to the reference 1.33 mm/rev, it corresponds to 9.8 N·m of cutting torque at 90 rpm/120 mm/min (9.2 N·m with $e = 0.83$). The measured values are 9.9 N·m for the reference pool and 10.5 N·m for record pda981. The measured mean torque is therefore consistent with the supplier's cutting data within 7%. This is a plausibility check of the torque channel and of the absolute level, not an independent validation of Equation (2): the supplier's calculation is itself a specific-force model, and the scaling uses the exponent of Equation (2). Peaks behave differently. The supplier's maximum-to-mean ratio, 1.24, reflects only the kinematic fluctuation of tooth engagement. The measured ratio of cutting torques, $(T_{m,99} - T_0)/(\overline{T}_m - T_0)$, is 2.5. The excess is dynamic amplification by the structure, the

gearbox backlash and tooth impacts, so peaks must be modelled from measurement. Each statistic q (mean or 99th percentile) is therefore anchored to the reference set:

$$T_{\mathrm{m},q}(n, v_\mathrm{f}) = T_0 + \left(T_{\mathrm{m},q}^{\mathrm{ref}} - T_0\right)\left(\frac{v_\mathrm{f}/n}{(v_\mathrm{f}/n)_{\mathrm{ref}}}\right)^{e_q} \quad (3)$$

with $(v_\mathrm{f}/n)_{\mathrm{ref}} = 120/90 = 1.33$ mm/rev and $T_0 = 1.4$ N·m (median no-load torque at 90 rpm). The exponent is identified from a feed step inside one record (pda981, Section 3.3). At 1 and 2 mm/s on the same wall, the segment means are 7.3 and 11.9 N·m, giving $e = 0.83$; the 99th percentiles are 14.3 and 29.5 N·m, giving $e = 1.12$. Peaks grow faster with feed than the mean does, as expected if the peak force follows the maximum chip thickness and excites the structure more strongly. Every prediction is evaluated for e in [0.75, 0.83] (mean) and [0.75, 1.12] (99th percentile), and the worst value is used.

2.5. Constraints and Ranking

A pair (n, v_f) is feasible if all three conditions hold:

- Vibration: n lies outside the resonant interval 75–88 rpm, defined by the 80 rpm record and the half-way points to its neighbours (the order analysis of Section 3.2 places the crossing at 77–87 rpm).
- Mean (thermal) torque: $\overline{T}_\mathrm{m}$ is at most the motor's $M_\mathrm{n} = 40$ N·m [40], and the gearbox output torque $\overline{T}_\mathrm{m}\, i\, \eta$ is at most $T_{2\mathrm{N}}$ [41]. Neither condition was active in the grid studied.
- Peak (jam) torque: $T_{\mathrm{m},99}$ is at most $T_{\mathrm{lim}} = 45$ N·m for every exponent in the range. T_{lim} is 9% below the lowest torque in that jam dataset (49.3 N·m on the thinner 35 mm wall). The process window itself remains for the 75 mm wall; 35 mm is only the empirical source of the fence. T_{lim} also equals the maximum torque reported in the site acceptance of continuous 75 mm cutting and corresponds to 39% of the gearbox's $T_{2\mathrm{B}}$. No jam was recorded on the 75 mm wall, so the limit is a motor-side fence for the 75 mm cut, not a measured jam threshold of that cut. It limits the 99th percentile of a steady segment. The reference set reaches a sample maximum of 49.2 N·m while its 99th percentile is 26.4 N·m, so a trip on every raw sample at 45 N·m would have stopped normal cutting. The 36 sensitivity cases vary the limit, the reference peak and the band definition. They do not vary tool wear, material scatter or frame stiffness.

The feeds studied are the PLC set-points 1–4 mm/s (60–240 mm/min); the speeds are the seven sweep speeds. Feasible pairs are ranked lexicographically: maximum MRR $= a_\mathrm{e}\, a_\mathrm{p}\, v_\mathrm{f}$ first, then minimum A_{band}. No weighted cost function is used [46], because the constraints are physical limits rather than preferences.

3. Results

3.1. Vibration Versus Spindle Speed

Table 5 and Figure 4 summarise the sweep. At 80 rpm the dominant line is 2.26 mm/s at 716 Hz, and $A_{\mathrm{band}} = 3.47$ mm/s is 98.8% of the broadband RMS (3.51 mm/s), i.e., 97.6% of the vibration energy lies in the band. At 110 rpm the same band carries 0.22 mm/s, a factor of 15.5 lower and the minimum of the sweep. The speeds of 100 and 120 rpm are nearly as quiet (0.39 and 0.30 mm/s), 60 and 70 rpm are intermediate (0.56 and 0.67 mm/s), and 90 rpm, the present production speed, lies on the flank of the resonance (0.51 mm/s).

Changing the band limits does not change which speed is quietest. For all five definitions the quietest speed is 110 rpm and the second is 120 rpm; only the order of 60, 70, 90 and 100 rpm changes. The window correction scales all values by the same factor and does not affect the ranking.

3.2. Order Analysis: A Forced-Resonance Interpretation

Table 6 and Figure 5 identify the excitation. Every spectrum contains a line whose frequency is proportional to n: 535, 626, 716, 807, 896, 987, 1077 Hz at 60–120 rpm. At 70–120 rpm its order is 539–541 times the spindle rotation frequency $f_s = n/60$, or 19.26–19.32 f_t. It is the strongest line between 400 and 1150 Hz at 70, 80, 100 and 110 rpm. Because its order is not an integer multiple of f_t, it is not a harmonic of tooth passing: at 80 rpm it lies 10.7 Hz (2.7 lines) above 19 f_t, more than the 8 Hz half-width of the Hanning main lobe [43]. Its source is most likely in the drive train, for example, a gear mesh, whose order relative to the output shaft is in general non-integer in a planetary gearbox. The gear data needed to confirm this are not available. The line crosses the 690–780 Hz band between 76.7 and 86.7 rpm, which reproduces the resonant interval of 75–88 rpm. Its amplitude rises from 0.42 mm/s at 70 rpm to 2.26 mm/s at 80 rpm and falls to 0.42 mm/s at 90 rpm (Figure 5b). In addition, lines at fixed frequencies between about 715 and 790 Hz appear at all speeds with small amplitude (below 0.5 mm/s), representing the response of the structural mode to the broadband cutting excitation.

Table 6. Order analysis of the sweep. n: speed displayed by the analyser. Dominant line: largest line of the spectrum (10–6400 Hz). Order line: the speed-locked component tracked between 400 and 1150 Hz (frequency refined by parabolic interpolation). Amplitudes are line values in mm/s RMS.

n (rpm)	f_s (Hz)	f_t (Hz)	Dominant Line (Hz)	f/f_t	A_{peak}	Order Line (Hz)	f/f_s	A (mm/s)
59.7	1.00	27.9	748	26.84	0.48	535	537.3	0.08
69.7	1.16	32.5	628	19.31	0.42	626	539.4	0.42
79.6	1.33	37.2	716	19.27	2.26	716	539.7	2.26
89.6	1.49	41.8	788	18.85	0.78	807	540.2	0.42
99.6	1.66	46.5	896	19.29	0.23	896	540.0	0.23
109.5	1.83	51.1	44	0.86	0.18	987	541.0	0.13
119.5	1.99	55.7	48	0.86	0.24	1077	541.1	0.06

The 80 rpm peak has the pattern expected of a forced resonance. We report it as an interpretation, because the natural frequency was not measured independently: a speed-locked excitation passes through a fixed structural mode. Regenerative chatter would appear near the mode frequency without locking to n and would grow with depth of cut rather than with the coincidence of an order and a mode [18,47]. Chatter cannot be excluded completely from single-block spectra; an impact test of the module, for which the analyser has a built-in function, would settle it, and operational modal analysis would give the damping [20,21]. Stability lobes were not computed. The order analysis also explains why a Campbell screen built on cutter-tooth harmonics alone would be misleading. The 19th harmonic lies in the band at 80 rpm, but so does the 14th harmonic at 110 rpm (715 Hz), where A_{band} is the lowest measured [16,48]. The band line at 110 rpm (764 Hz, 0.11 mm/s) is a weak 15th tooth harmonic. At 100–120 rpm the largest line below 400 Hz lies at 40, 44 and 48 Hz. This is 24.1 f_s (0.86 f_t), again speed-locked but not at tooth passing; its source has not been identified.

3.3. Measured Spindle Torque

Figure 6 shows the feed step in record pda981. At constant 90 rpm the spindle torque settles at 7.3 N·m for 1 mm/s and at 11.9 N·m for 2 mm/s; with the feed stopped, it returns to the no-load level of 1.4 N·m. The step is immediate and reversible, which confirms that T_m responds to chip load, as expected for drive-signal force estimation [27,28]. Table 7 lists the statistics used in the model.

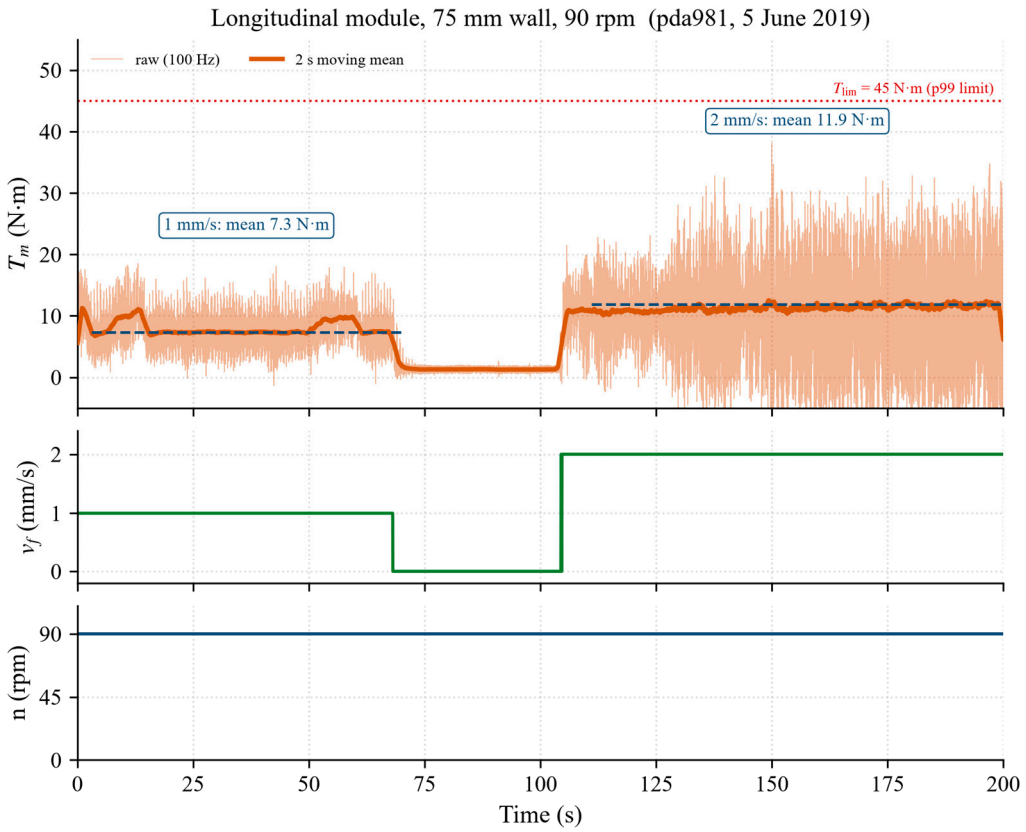

Figure 6. Feed step during cutting of the 75 mm wall by the longitudinal module (pda981, 5 June 2019). (**Top**): spindle-motor torque, raw (100 Hz) and 2 s moving mean; dashed: segment means. (**Middle**): feed speed. (**Bottom**): spindle speed.

Table 7. Spindle-motor torque statistics at 90 rpm (N·m), duration-weighted over segments. Jams: torque immediately before the speed collapse.

Data Set	Segments	Cut Time (s)	$T_0/\bar{T}_m$	$T_{m,95}$	$T_{m,99}$	$T_{m,max}$
No load, 90 rpm, feed stopped	–	–	1.4	–	–	–
pda981, 1 mm/s	3	46	7.3	12.3	14.3	18.0
pda981, 2 mm/s	5	275	11.9	24.7	29.5	45.5
Reference: 75 mm, 2 mm/s (June + December 2019)	65	2064	11.3	22.1	26.4	49.2
ISCAR MP, scaled to 90 rpm/ 120 mm/min	–	–	11.2	–	–	–
pda148, 2 mm/s (reduced depth)	–	217	8.6	–	34.4	–
pda148, 4 mm/s, first 29 s (not fitted)	–	29	12.2	–	36.9	–
Jam dataset only (thinner 35 mm wall), 1.0–1.2 mm/s	5 events	–	–	–	–	49.3–68.2

Figure 7 places the data on the feed-per-revolution axis of Equation (3). The reference pool and pda981 fall on the identified mean-torque band; the supplier's value at 2.8 mm/rev lies about 1% below its lower edge. The segment-to-segment spread of the mean (q10–q90 5.4–16.6 N·m) is larger than the model band, mainly because entry and exit cuts are included.

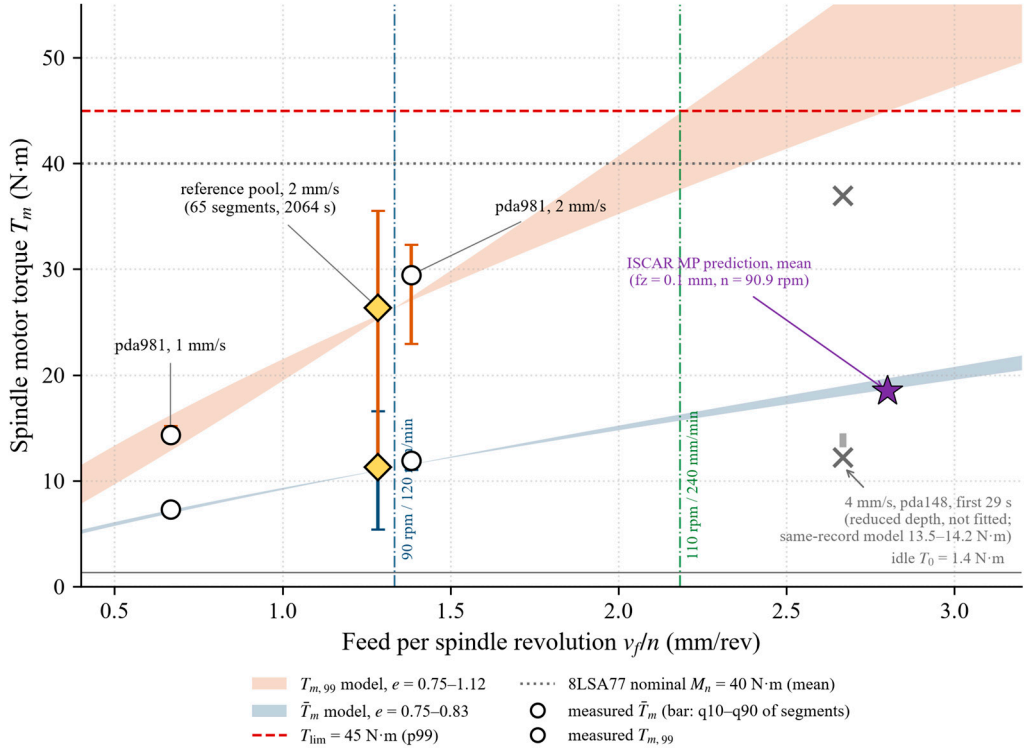

Figure 7. Spindle-motor torque versus feed per revolution. Bands: Equation (3) for the mean (blue, e = 0.75–0.83) and the 99th percentile (orange, e = 0.75–1.12). Markers: measured, bars q10–q90 of segment values; star: ISCAR MP mean torque referred to the motor; crosses: pda148 at 4 mm/s (reduced depth) with the same-record prediction (grey bar). Vertical lines: current and selected operating points.

The only cut at 4 mm/s is in record pda148 (16 December 2019, 90 rpm): 217 s at 2 mm/s followed by 149 s at 4 mm/s over 600 mm of feed travel. Its 2 mm/s part has a mean torque of 8.6 N·m against 11.3 N·m in the reference pool, so the radial engagement was smaller than the full wall. Scaled from this part with Equation (3), the mean torque at 4 mm/s should be 13.5–14.2 N·m. The first 29 s at 4 mm/s gave 12.2 N·m ($T_{m,99}$ = 36.9 N·m), 9–14% below the prediction; later 30 s windows fell to 6.4–9.6 N·m as the engagement decreased further. The record is therefore not used for fitting. It does, however, check the doubling of feed within one record, and it shows that 4 mm/s was run at 90 rpm without a jam.

Figure 8 shows why the peak limit is set by jams rather than by the motor. Before the jam in pda847 (thinner 35 mm wall; used only as the source of T_{lim}), the 0.8 s mean torque is about 7 N·m and isolated peaks reach 45–55 N·m. Immediately before the collapse the mean rises to 29 N·m and the raw signal reaches 68 N·m, while n is still 90 rpm. The motor could deliver far more (M_{max} = 270 N·m). The stall is mechanical (the cutter seizes in the kerf), and the torque rise is its precursor, the kind of event that drive-signal monitoring is designed to catch [31,49].

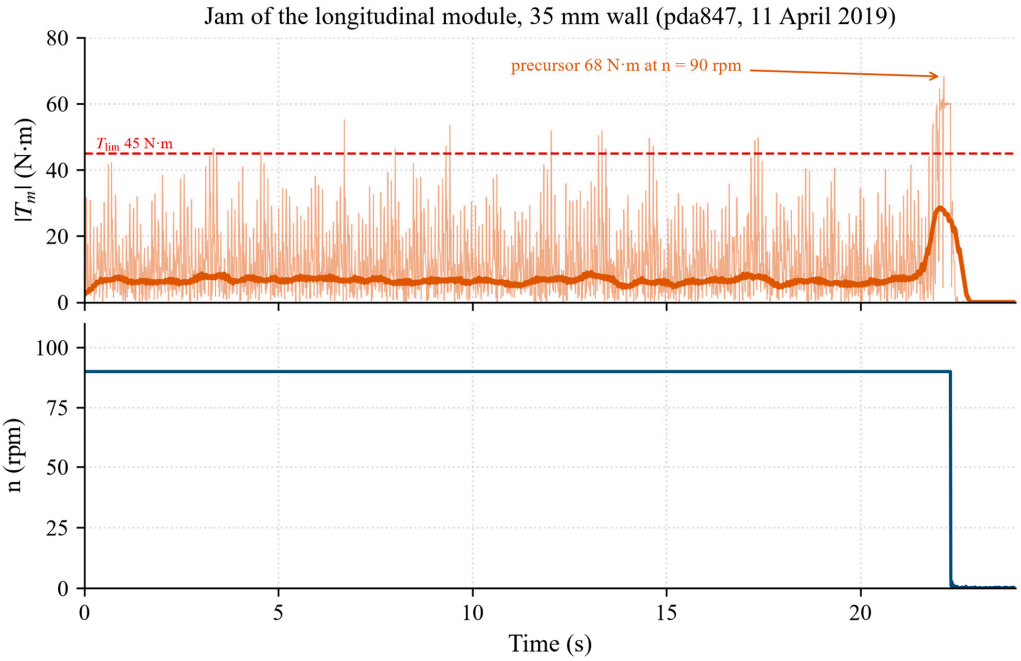

Figure 8. Jam precursor used only to set T_{lim} (thinner 35 mm wall, pda847, 11 April 2019). (**Top**): $|T_m|$ raw and 0.8 s moving mean. (**Bottom**): spindle speed.

3.4. Process Window

Figure 9 puts both constraints on the speed axis. Panel (a) is the test-stand measurement. In panel (b) the curves are the torque model; the reference marker and the jam range are measured. Vibration (a) is a narrow function of n. Torque (b) is a smooth, falling function of n at each feed, because raising n at constant v_f reduces the chip thickness. Figure 10 and Table 8 give the resulting window. Six feasible cells exceed the current MRR: 90–120 rpm at 3 mm/s and 110–120 rpm at 4 mm/s (60–70 rpm fail the peak limit already at 3 mm/s). At 4 mm/s, 90 and 100 rpm violate the peak limit for the upper exponent ($T_{m,99}$ up to 56 and 50 N·m). The maximum feasible MRR, 108 cm^3/min, is reached only at 110 and 120 rpm with 240 mm/min, and the test-stand value of A_{band} breaks the tie in favour of 110 rpm.

Table 8. Selected cells of the (n, v_f) grid. Torque ranges span the exponent ranges of Equation (3); a single value is given where the range rounds to one number (at the reference point the model reproduces the measurement). MRR = $a_e\, a_p\, v_f$ with a_e = 75 mm and a_p = 6 mm.

n (rpm)	v_f (mm/min)	A_{band} (mm/s)	$\bar{T}_m$ (N·m)	$T_{m,99}$ (N·m)	MRR (cm^3/min)	Status
90	120	0.51	11	26	54	current production (measured reference)
80	180	3.47	16–17	38–46	81	resonance
90	180	0.51	15	35–41	81	feasible
110	180	0.22	13	31–33	81	feasible, largest torque margin at 3 mm/s
90	240	0.51	18–19	43–56	108	peak torque > 45 N·m
100	240	0.39	17–18	40–50	108	peak torque > 45 N·m (upper e)

Table 8. *Cont.*

n (rpm)	v_f (mm/min)	A_{band} (mm/s)	$\bar{T}_m$ (N·m)	$T_{m,99}$ (N·m)	MRR (cm³/min)	Status
110	240	0.22	16	38–45	108	selected
120	240	0.30	15	35–41	108	feasible; more torque margin

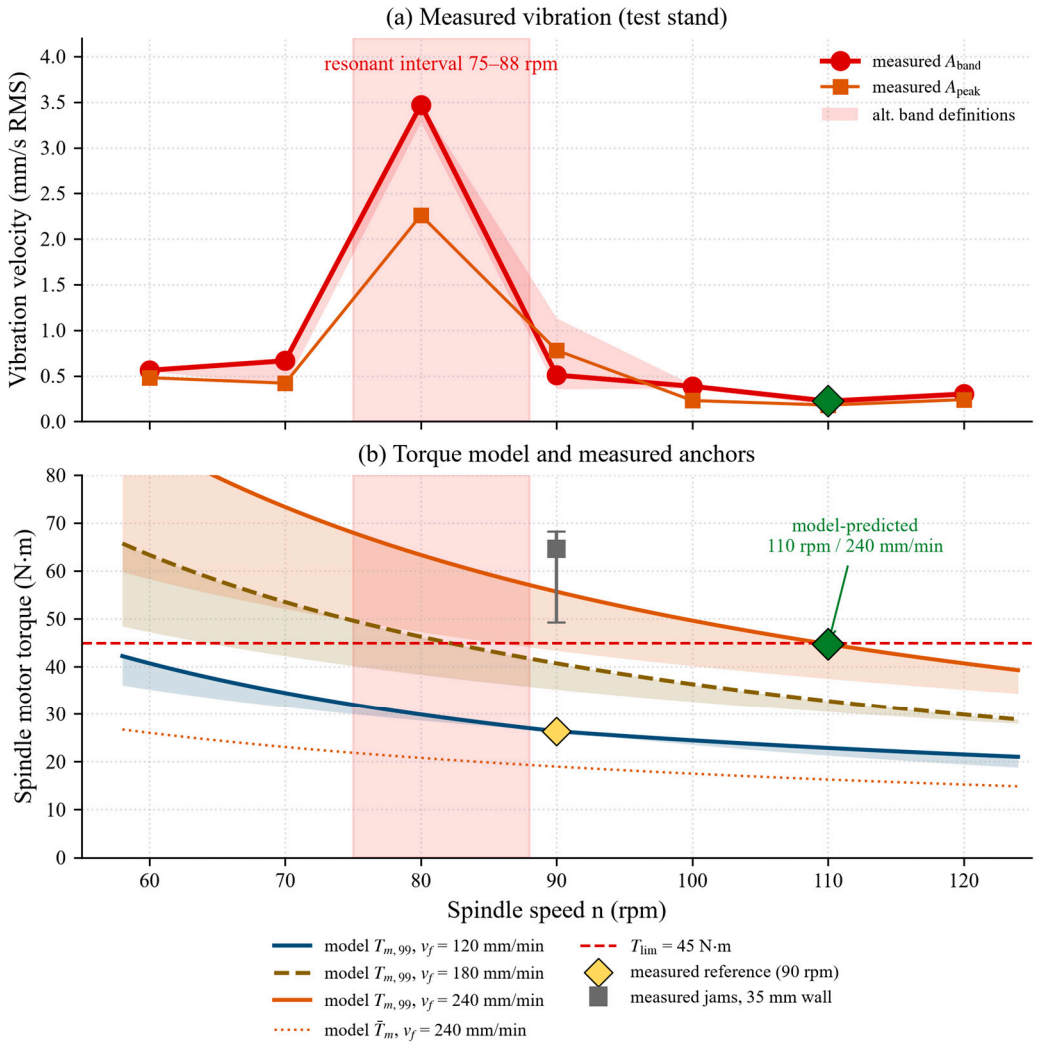

Figure 9. Plotted from the measurements and from Equation (3). (**a**) Measured A_{band} and A_{peak} versus spindle speed; the light band spans the alternative band definitions. (**b**) Predicted $T_{m,99}$ at three feeds (line: upper exponent; shading: exponent range), mean torque at 240 mm/min, the 45 N·m limit, the measured reference and the range of the five jam torques from the thinner-wall jam dataset (35 mm; source of T_{lim} only).

3.5. Sensitivity of the Decision

The decision was recomputed for 36 combinations: peak limit 40, 45 or 49.3 N·m; reference peak torque scaled by 0.9, 1.0 or 1.1; and four band definitions. The condition 110 rpm/240 mm/min is selected in 20 cases, 120 rpm/240 mm/min is selected in 8 (reference peak 10% higher at T_{lim} = 45 N·m, or 10% lower at T_{lim} = 40 N·m), and 110 rpm/180 mm/min in 8 (T_{lim} = 40 N·m with nominal or higher reference peak). The band definition never changes the result. The selected speed is therefore 110–120 rpm in every case, and the feed is 240 mm/min unless the peak limit is tightened to 40 N·m. At the upper exponent,

110 rpm/240 mm/min lies within 0.3 N·m of T_{lim}, so the modelled reserve at that edge is zero. The point should be introduced with an alarm on the measured torque. A prediction below 45 N·m does not itself protect the cut. The alarm belongs on a short-window mean or percentile, read while the speed is still at the set-point. A trip on every raw sample at 45 N·m would have stopped normal 75 mm cutting: the reference set reaches a sample maximum of 49.2 N·m while its 99th percentile stays at 26.4 N·m. Figure 8 shows the jam precursor as a rise in the short-window mean, not as a single sample. The filter length is not yet fixed. The condition 120 rpm/240 mm/min, which is 3360 rpm at the motor and still below the gearbox nominal input speed, gives the same removal rate with about 4 N·m more margin and is the fallback. The removal rate of 108 cm^3/min belongs to the 45 N·m limit. When the limit is 40 N·m and the reference peak is not reduced, the selected feed falls to 180 mm/min and the removal rate is 81 cm^3/min.

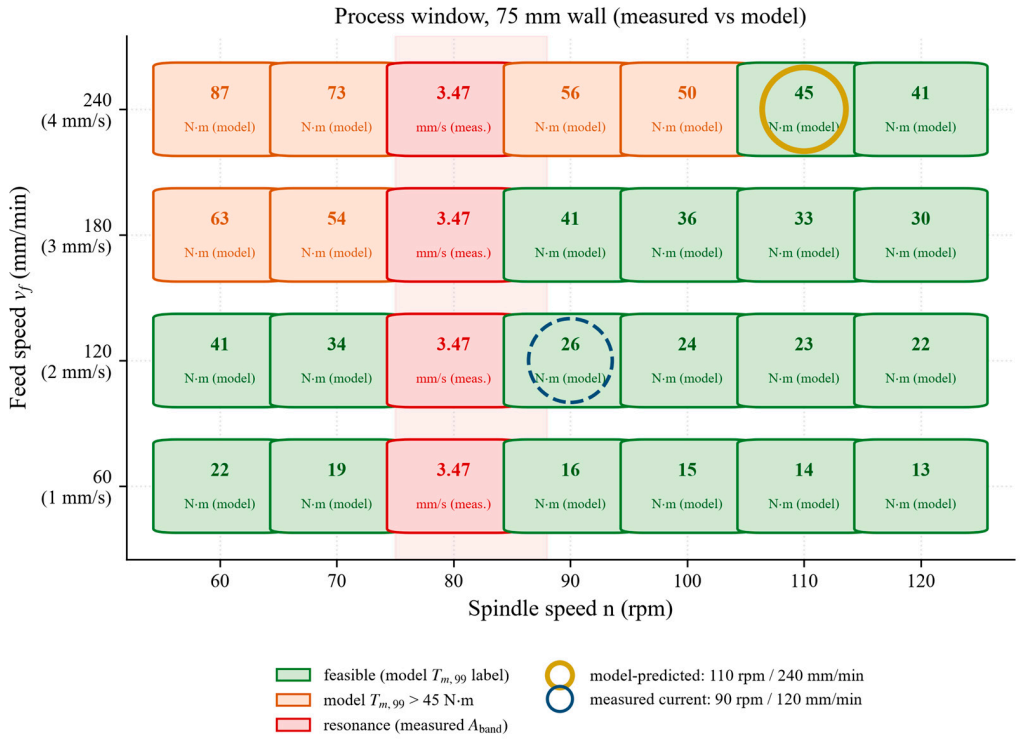

Figure 10. Process window for the 75 mm wall ($z = 28$). Cell label: upper bound of $T_{m,99}$ over the exponent range (N·m), or A_{band} (mm/s) in the resonant interval. Gold ring: model-predicted feasible point. Dashed ring: measured current production. Red cells report the measured band value. Green and orange cells report the model.

4. Discussion

4.1. Gain and Operating Margins

Relative to the current practice (90 rpm, 120 mm/min), the model-predicted condition doubles the kinematic MRR from 54 to 108 cm^3/min, reduces A_{band} from 0.51 to 0.22 mm/s (−56%) and moves the 99th-percentile torque from 26 N·m to at most 45 N·m. The mean torque rises from 11 to 16 N·m, 40% of the motor's nominal torque; at 3080 rpm this is 5.3 kW against a nominal power of 12.6 kW [40]. At the cutter it is about 430 N·m, 21% of the gearbox's T_{2N} [41]. The vibration values were measured on the test stand and were not repeated at 240 mm/min. The torque at 110 rpm is an extrapolation of Equation (3). The thermal limits lie far from the predicted mean, and the active constraint is the jam-related peak. The gain in MRR exceeds what a pure feed increase would allow, because raising n from 90 to 110 rpm reduces the chip thickness by 18% at a given v_f, and the torque reserve

gained is then spent on feed. The in-cut time per metre of kerf falls from 8.3 to 4.2 min. For the twelve generators of the plant, cutting time was one of the components of the 45-day cycle per generator [36], and time spent by the crew near the component is the main lever on dose [4]; the share of in-cut time in that cycle was not recorded, so the saving is not converted into days or dose here.

The supplier's operating point (90.9 rpm, f_z = 0.1 mm, 254.5 mm/min, 114.5 cm^3/min) illustrates the difference between a power check and a field window. Its mean motor torque, 18 N·m, is acceptable, but Equation (3) predicts a 99th-percentile torque of 45–59 N·m, which reaches the jam range. The selected point achieves 94% of that MRR at a lower feed per tooth (0.078 mm) by moving to 110 rpm, where the test-stand spectrum is the quietest of the seven speeds. A catalogue optimisation in the sense of Taylor-type or energy-based criteria [33,50] would see neither the resonance nor the dynamic amplification of peaks.

The drive train adds a protection requirement that the window alone does not show. The motor's peak torque of 270 N·m corresponds to about 7100 N·m at the gearbox output, 1.2 times the gearbox's emergency-stop torque (6045 N·m) [40,41]. The spindle drive's torque limit must therefore be set from the gearbox side, at no more than $T_{2B}/(i\,\eta)$ = 115 N·m on the motor. The jam torques observed so far (at most 68 N·m) lie below this value. With the 45 N·m alarm on $T_{m,99}$ there is a margin of about 70 N·m between warning and gearbox limit.

4.2. Chip Evacuation, Cutting Speed and Tool Wear

In dry slitting of a 75 mm wall, the chip must leave the 6 mm kerf in the tooth gullet, and packing of chips in the kerf is a usual cause of seizure. The selected point does not increase the gullet load: the chip volume per tooth, $f_z\ a_e$ CW, is 35 mm^3 at 110 rpm/240 mm/min, against 21 mm^3 in the current practice and 45 mm^3 at the supplier's design point (f_z = 0.1 mm). The five jam events used only to set T_{lim} occurred on a thinner (35 mm) wall; their cause was not documented. Chip packing and closure of the kerf by release of residual stresses are the usual candidates, and both depend on the wall rather than on n. They did not occur on the 75 mm wall even at 4 mm/s (pda148).

The cutting speed rises from v_c = 119 m/min at 90 rpm to 145 m/min at 110 rpm (158 m/min at 120 rpm), against 120 m/min in the supplier's calculation. Tool life was not measured. With a Taylor exponent of 0.25, typical of carbide in low-carbon steel [33], tool life in minutes would fall to about 45% of the present value. Because the MRR doubles, the volume removed per tool life would remain about 90% of the present value. This is an estimate with an assumed exponent, not a measurement. If the exponent is steeper, or if dry cutting at 145 m/min damages the edge by some other mechanism, part of the time saving is spent on tool changes. Edge wear should be inspected after the first validation cuts. Dry cutting is used here because the chip is solid and no contaminated coolant is produced. Energy per unit volume was not measured, so that choice is an operational reason rather than a measured environmental gain.

4.3. Method and Limitations

The result also shows that the two common shortcuts fail on this machine. A torque-only sizing would accept 80 rpm, the worst speed dynamically. A Campbell screen based on tooth harmonics would reject 110 rpm, the best one, whereas the measured order spectrum shows which excitation actually reaches the mode. Only the combination of a measured speed series and a measured load map gives a defensible window. For field equipment both are cheap: one analyser session and the drive log that the PLC writes anyway. Drive-signal monitoring is established in machining research [51,52]. Here the same signal also serves

as the calibration source, and its 99th percentile is a better peak-load measure than the maximum, which is dominated by single events.

The limitations are stated explicitly:

- The model-predicted point has not yet been run in production. The torque at 110 rpm is a prediction of Equation (3). The feed step and the 4 mm/s cut support the feed dependence at 90 rpm. The supplier's calculation checks the torque level at the reference condition. It does not check the exponent, and it does not check the change in speed. A validation run at 110 rpm with a feed step of 1–2–3–4 mm/s, the torque alarm at 45 N·m and a simultaneous vibration record is the next step, and it would also refine the exponent identified from one 46 s feed step.
- Vibration was measured on the first version of the longitudinal module on a test stand; torque was logged on the module installed in the cell. Spindle drive, gearbox and cutter are the same, but clamping and frame stiffness differ [19]. The resonant interval should be confirmed in the cell with a short sweep at 80, 90 and 110 rpm and an impact test. Until those records exist, 110 rpm is the quietest speed of the test stand. It is not a demonstrated minimum of the installed module, because a change of frame stiffness moves the speed at which the order meets the mode.
- Each spectrum is a single 0.25 s block from one accelerometer in one direction at one feed. A_{band} is assumed independent of v_{f} at a quiet speed; this is plausible for forced vibration far from resonance but untested at 240 mm/min.
- Torque at speeds other than 90 rpm is extrapolated through Equation (3). The extrapolation assumes no speed effect on k_{c} in the range 90–120 rpm (v_{c} = 119–158 m/min) [26].
- The peak limit T_{lim} uses jam precursors from a thinner (35 mm) wall as its empirical source only. The process window is for the 75 mm wall, where no jam occurred; the jam mechanism was not identified.
- The gear ratio $i = 28$ enters only the cutter-side torques and the motor speeds; motor-side results do not depend on it.
- The speed-locked components at 540 f_{s} and 24.1 f_{s} have not been assigned to a machine element.
- The 530 mm, 36-tooth cutter used on the 135–140 mm wall has a different tooth-passing ladder and a different load; the window does not transfer to it without a new sweep.

5. Conclusions

A process window for dry disc milling of the 75 mm shell of VVER-440 steam generators by the longitudinal cutting module was built from a seven-speed vibration sweep and 599 records of the cell's drive log.

- Vibration depends on spindle speed. A 690–780 Hz band makes 75–88 rpm unusable (A_{band} = 3.47 mm/s at 80 rpm). Order tracking shows a speed-locked drive-train order (540 f_{s}) crossing a fixed structural mode, read as a forced-resonance interpretation, not as a measured natural frequency. On the test stand, 110 rpm is the quietest speed (0.22 mm/s) for every band definition tested.
- Spindle torque depends on feed per revolution. At the reference condition the measured mean torque is consistent within 7% with the tool supplier's cutting-power calculation. That figure checks the level, not the exponent; the mean scales with exponent 0.83 and the 99th percentile with 1.12. Peak cutting torque is 2.5 times the mean, against 1.24 predicted kinematically, so peaks must be taken from measurement.
- The thermal limits of motor and gearbox are never active; the binding limit is the peak torque that precedes a jam (49–68 N·m in five events from the thinner-wall jam dataset, used only to set T_{lim} for the 75 mm window). A 45 N·m limit on the 99th percentile is

proposed. The limit applies to the percentile, not to every sample. The drive's torque limit should not exceed about 115 N·m to protect the gearbox.

- The model-predicted feasible condition is 110 rpm/240 mm/min (4 mm/s): MRR 108 cm^3/min, twice the current practice, with 56% less resonant-band vibration on the test stand and a lower chip load per tooth than the supplier's design point. The condition 120 rpm/240 mm/min is the alternative with more torque margin. The doubled removal rate belongs to the 45 N·m limit; at 40 N·m, the selected feed falls to 180 mm/min. A validation run at 110 rpm is the next step.
- The method needs only a portable analyser and the PLC drive log, and it can be repeated whenever the cutter, wall thickness or module changes.

6. Patents

The fragmentation device of which the longitudinal cutting module is part is described in European patent application EP 3 984 674 A1, Device for fragmenting large cylindrical containers (application No. EP21203183.5), and protected by Slovak utility model No. 9250 [38].

Author Contributions: Conceptualization, J.V. and J.S.; methodology, J.V.; software, J.V. and P.P.; validation, J.V., P.P. and O.Š.; formal analysis, J.V.; investigation, J.V. and P.P.; resources, J.S.; data curation, J.V.; writing—original draft preparation, J.V.; writing—review and editing, J.S., P.P., B.J. and O.Š.; visualization, J.V.; supervision, J.S.; project administration, J.V.; funding acquisition, J.S. All authors have read and agreed to the published version of the manuscript.

Funding: This research was funded by the European Union's Horizon Europe research and innovation programme under grant agreement No. 101104241 (project REBELION—Research and development of a highly automated and safe streamlined process for increased Lithium-ion battery repurposing and recycling). Call: HORIZON-CL5-2022-D2-01; topic: HORIZON-CL5-2022-D2-01-10; type of action: HORIZON-RIA.

Institutional Review Board Statement: Not applicable.

Informed Consent Statement: Not applicable.

Data Availability Statement: The original contributions presented in this study are included in the article. Further inquiries can be directed to the corresponding author. The seven velocity spectra (CSV export of the analyser), the analyser screens, the segment statistics (424 segments), the event classification and the scripts used to decode the ibaPDA records and build the window are available from the corresponding author upon reasonable request, subject to the confidentiality conditions of the decommissioning project.

Acknowledgments: The authors thank colleagues at the Prototyping and Innovation Centre, Technical University of Košice, for laboratory support during the physical experiments.

Conflicts of Interest: J.V. is a co-inventor of the device described in European patent application EP 3 984 674 A1. The other authors declare no conflicts of interest.

Abbreviations

The following abbreviations and symbols are used in this manuscript:

ENBW	Equivalent noise bandwidth
FFT	Fast Fourier transform
MRR	Material-removal rate (cm^3/min)
NPP	Nuclear power plant
PGV-4E	Horizontal steam generator of the VVER-440 reactor
PLC	Programmable logic controller
RMS	Root mean square
VVER	Water-cooled, water-moderated power reactor

A_{band}	Band RMS of the velocity spectrum in 690–780 Hz, Equation (1) (mm/s)
A_{peak}	Dominant-line amplitude of the spectrum (mm/s)
a_e, a_p	Radial depth (wall thickness), axial depth (cutter width) (mm)
D_C, z	Cutter diameter (mm), number of teeth
e	Feed-per-revolution exponent of torque, Equation (3)
f_s, f_t	Spindle rotation frequency $n/60$; tooth-passing frequency $n\,z/60$ (Hz)
h_m	Mean uncut chip thickness (mm)
i, η	Spindle gear ratio (28), gearbox efficiency (0.94)
k_c, $k_{c1.1}$, m_c	Specific cutting force (N/mm^2); Kienzle constant and exponent
M_n, M_0, M_{max}	Nominal, stall and peak torque of the spindle motor (N·m)
n	Spindle (gearbox-output) speed (rpm)
T_0	No-load spindle-motor torque at 90 rpm (N·m)
T_{2N}, T_{2B}, T_{2NOT}	Gearbox nominal, max. acceleration and emergency-stop output torque (N·m)
T_m, $\overline{T}_m$, $T_{m,99}$	Spindle-motor torque; segment mean; segment 99th percentile (N·m)s
T_{lim}	Peak-torque limit applied to $T_{m,99}$, 45 N·m
v_c	Cutting speed $\pi\,D_C\,n$ (m/min)
v_f	Feed speed (PLC set-point in mm/s; 1 mm/s = 60 mm/min)

References

1. Volk, R.; Hübner, F.; Hünlich, T.; Schultmann, F. The future of nuclear decommissioning—A worldwide market potential study. *Energy Policy* **2019**, *124*, 226–261. [CrossRef]
2. IAEA. *State of the Art Technology for Decontamination and Dismantling of Nuclear Facilities*; Technical Reports Series No. 395; International Atomic Energy Agency: Vienna, Austria, 1999.
3. Invernizzi, D.C.; Locatelli, G.; Velenturf, A.; Love, P.E.D.; Purnell, P.; Brookes, N.J. Developing policies for the end-of-life of energy infrastructure: Coming to terms with the challenges of decommissioning. *Energy Policy* **2020**, *144*, 111677. [CrossRef]
4. Shin, J.; Lee, D.; Ahn, S.; Cho, D.-W. A study on the optimization through the evaluation of radiation exposure by scenarios during steam generator dismantling. *Ann. Nucl. Energy* **2024**, *211*, 110901. [CrossRef]
5. Lee, G.-R.; Lim, B.-J.; Cho, D.-W.; Park, C.-D. Selection methodology of the optimal cutting technology for dismantling of components in nuclear power plants. *Ann. Nucl. Energy* **2022**, *166*, 108808. [CrossRef]
6. Sreejith, P.S.; Ngoi, B.K.A. Dry machining: Machining of the future. *J. Mater. Process. Technol.* **2000**, *101*, 287–291. [CrossRef]
7. Weinert, K.; Inasaki, I.; Sutherland, J.W.; Wakabayashi, T. Dry machining and minimum quantity lubrication. *CIRP Ann.* **2004**, *53*, 511–537. [CrossRef]
8. Zhu, L.; Liu, C. Recent progress of chatter prediction, detection and suppression in milling. *Mech. Syst. Signal Process.* **2020**, *143*, 106840. [CrossRef]
9. Merritt, H.E. Theory of self-excited machine-tool chatter: Contribution to machine-tool chatter research—1. *J. Eng. Ind.* **1965**, *87*, 447–454. [CrossRef]
10. Altintas, Y.; Budak, E. Analytical prediction of stability lobes in milling. *CIRP Ann.* **1995**, *44*, 357–362. [CrossRef]
11. Altintas, Y.; Weck, M. Chatter stability of metal cutting and grinding. *CIRP Ann.* **2004**, *53*, 619–642. [CrossRef]
12. Insperger, T.; Stépán, G. Semi-discretization method for delayed systems. *Int. J. Numer. Methods Eng.* **2002**, *55*, 503–518. [CrossRef]
13. Ding, Y.; Zhu, L.; Zhang, X.; Ding, H. A full-discretization method for prediction of milling stability. *Int. J. Mach. Tools Manuf.* **2010**, *50*, 502–509. [CrossRef]
14. Davies, M.A.; Pratt, J.R.; Dutterer, B.; Burns, T.J. Stability prediction for low radial immersion milling. *J. Manuf. Sci. Eng.* **2002**, *124*, 217–225. [CrossRef]
15. Merdol, S.D.; Altintas, Y. Multi frequency solution of chatter stability for low immersion milling. *J. Manuf. Sci. Eng.* **2004**, *126*, 459–466. [CrossRef]
16. Altintas, Y. *Manufacturing Automation: Metal Cutting Mechanics, Machine Tool Vibrations, and CNC Design*, 2nd ed.; Cambridge University Press: Cambridge, UK, 2012.
17. Munoa, J.; Beudaert, X.; Dombovari, Z.; Altintas, Y.; Budak, E.; Brecher, C.; Stepan, G. Chatter suppression techniques in metal cutting. *CIRP Ann.* **2016**, *65*, 785–808. [CrossRef]
18. Navarro-Devia, J.H.; Chen, Y.; Dao, D.V.; Li, H. Chatter detection in milling processes—A review on signal processing and condition classification. *Int. J. Adv. Manuf. Technol.* **2023**, *125*, 3943–3980. [CrossRef]
19. Brecher, C.; Esser, M.; Witt, S. Interaction of manufacturing process and machine tool. *CIRP Ann.* **2009**, *58*, 588–607. [CrossRef]
20. Zaghbani, I.; Songmene, V. Estimation of machine-tool dynamic parameters during machining operation through operational modal analysis. *Int. J. Mach. Tools Manuf.* **2009**, *49*, 947–957. [CrossRef]
21. Brincker, R.; Zhang, L.; Andersen, P. Modal identification of output-only systems using frequency domain decomposition. *Smart Mater. Struct.* **2001**, *10*, 441–445. [CrossRef]

22. Thaler, T.; Potočnik, P.; Bric, I.; Govekar, E. Chatter detection in band sawing based on discriminant analysis of sound features. *Appl. Acoust.* **2014**, *77*, 114–121. [CrossRef]
23. Merchant, M.E. Mechanics of the metal cutting process. I. Orthogonal cutting and a type 2 chip. *J. Appl. Phys.* **1945**, *16*, 267–275. [CrossRef]
24. Biró, I.; Szalay, T. Extension of empirical specific cutting force model for the process of fine chip-removing milling. *Int. J. Adv. Manuf. Technol.* **2017**, *88*, 2735–2743. [CrossRef]
25. Budak, E.; Altintas, Y.; Armarego, E.J.A. Prediction of milling force coefficients from orthogonal cutting data. *J. Manuf. Sci. Eng.* **1996**, *118*, 216–224. [CrossRef]
26. Kaymakci, M.; Kilic, Z.M.; Altintas, Y. Unified cutting force model for turning, boring, drilling and milling operations. *Int. J. Mach. Tools Manuf.* **2012**, *54–55*, 34–45. [CrossRef]
27. Altintas, Y. Prediction of cutting forces and tool breakage in milling from feed drive current measurements. *J. Eng. Ind.* **1992**, *114*, 386–392. [CrossRef]
28. Kim, T.Y.; Kim, J. Adaptive cutting force control for a machining center by using indirect cutting force measurements. *Int. J. Mach. Tools Manuf.* **1996**, *36*, 925–937. [CrossRef]
29. Soliman, E.; Ismail, F. Chatter detection by monitoring spindle drive current. *Int. J. Adv. Manuf. Technol.* **1997**, *13*, 27–34. [CrossRef]
30. Aslan, D.; Altintas, Y. On-line chatter detection in milling using drive motor current commands extracted from CNC. *Int. J. Mach. Tools Manuf.* **2018**, *132*, 64–80. [CrossRef]
31. Teti, R.; Jemielniak, K.; O'Donnell, G.; Dornfeld, D. Advanced monitoring of machining operations. *CIRP Ann.* **2010**, *59*, 717–739. [CrossRef]
32. Mohamed, A.; Hassan, M.; M'Saoubi, R.; Attia, H. Tool condition monitoring for high-performance machining systems—A review. *Sensors* **2022**, *22*, 2206. [CrossRef] [PubMed]
33. Taylor, F.W. On the art of cutting metals. *Trans. ASME* **1907**, *28*, 31–350. [CrossRef]
34. Kara, S.; Li, W. Unit process energy consumption models for material removal processes. *CIRP Ann.* **2011**, *60*, 37–40. [CrossRef]
35. IAEA. Slovakia sets global example for nuclear power plant decommissioning. *IAEA Bull.* **2023**, *64*, 10–11. Available online: https://www.iaea.org/bulletin/slovakia-sets-global-example-for-nuclear-power-plant-decommissioning (accessed on 2 October 2026).
36. Vargovčík, L.; Varga, J.; Semjon, J. Robotic system for fragmentation of steam generators (StarGate). *EPJ Nucl. Sci. Technol.* **2026**, *12*, 9. [CrossRef] [PubMed]
37. Vargovčík, L.; Holcer, R.; Medved, J. Mobile robotic systems for fragmentation of nuclear equipment. *Appl. Mech. Mater.* **2013**, *282*, 116–122. [CrossRef]
38. Vargovčík, L.; Varga, J.; Vrabeľ, M.; Štubňa, M.; Kravárik, K.; Ondra, F. Device for Fragmenting Large Cylindrical Containers. European Patent Application EP 3 984 674 A1, 20 April 2022.
39. *GOST 5520-2017*; Rolled Sheet of Non-Alloy and Alloy Steel for Boilers and Pressure Vessels. Specifications. Standartinform: Moscow, Russia, 2017.
40. B&R Industrial Automation. *8LS…-3 Three-Phase Synchronous Motors*; User's Manual V2.51; B&R: Eggelsberg, Austria, 2018.
41. Apex Dynamics. *AP/APK/APC/APCK Series Planetary Gearboxes*; Catalogue; Apex Dynamics Inc.: Taichung, Taiwan, 2024; Available online: http://www.apexdynamics.it/wp-content/uploads/AP_APK_APC-APCK-2024-07-Eng.pdf (accessed on 9 October 2026).
42. Adash spol. s r.o. *A4400 VA4 Pro—Four-Channel Vibration Analyser, Data Collector and Recorder*; User Manual; Adash spol. s r.o.: Ostrava, Czech Republic, 2021; Available online: https://adash.com/documents/A4400/Adash-A4400-VA4-Pro-manual.pdf (accessed on 12 October 2026).
43. Harris, F.J. On the use of windows for harmonic analysis with the discrete Fourier transform. *Proc. IEEE* **1978**, *66*, 51–83. [CrossRef]
44. Randall, R.B. *Vibration-Based Condition Monitoring: Industrial, Aerospace and Automotive Applications*; Wiley: Chichester, UK, 2011.
45. *ISO 20816-3:2022*; Mechanical Vibration—Measurement and Evaluation of Machine Vibration—Part 3: Industrial Machines with a Power Rating Above 15 kW and Operating Speeds Between 120 r/min and 30 000 r/min. ISO: Geneva, Switzerland, 2022.
46. Yan, J.; Li, L. Multi-objective optimization of milling parameters—The trade-offs between energy, production rate and cutting quality. *J. Clean. Prod.* **2013**, *52*, 462–471. [CrossRef]
47. Quintana, G.; Ciurana, J. Chatter in machining processes: A review. *Int. J. Mach. Tools Manuf.* **2011**, *51*, 363–376. [CrossRef]
48. Schmitz, T.L.; Smith, K.S. *Machining Dynamics: Frequency Response to Improved Productivity*, 2nd ed.; Springer: Cham, Switzerland, 2019.
49. Byrne, G.; Dornfeld, D.; Inasaki, I.; Ketteler, G.; König, W.; Teti, R. Tool condition monitoring (TCM)—The status of research and industrial application. *CIRP Ann.* **1995**, *44*, 541–567. [CrossRef]

50. Mativenga, P.T.; Rajemi, M.F. Calculation of optimum cutting parameters based on minimum energy footprint. *CIRP Ann*. **2011**, *60*, 149–152. [CrossRef]
51. Liang, S.Y.; Hecker, R.L.; Landers, R.G. Machining process monitoring and control: The state-of-the-art. *J. Manuf. Sci. Eng*. **2004**, *126*, 297–310. [CrossRef]
52. Stavropoulos, P.; Chantzis, D.; Doukas, C.; Papacharalampopoulos, A.; Chryssolouris, G. Monitoring and control of manufacturing processes: A review. *Procedia CIRP* **2013**, *8*, 421–425. [CrossRef]

Disclaimer/Publisher's Note: The statements, opinions and data contained in all publications are solely those of the individual author(s) and contributor(s) and not of MDPI and/or the editor(s). MDPI and/or the editor(s) disclaim responsibility for any injury to people or property resulting from any ideas, methods, instructions or products referred to in the content.